IL NUOVO CIMENTO Vol. 34 C, N. 4 Luglio-Agosto 2011
DOI 10.1393/ncc/i2011-10957-y

Colloquia: Channeling 2010

Electromagnetic field features at interaction of relativistic electron with matter

G. A. Naumenko, L. G. Sukhikh, Yu. A. Popov and M. V. Shevelev

Physical and Technical institute, Tomsk Polytechnic University - Lenin Ave. 2a 634050 Tomsk, Russia

(ricevuto il 22 Dicembre 2010; pubblicato online il 12 Settembre 2011)

Summary. — The features of electromagnetic field of relativistic electrons passing through a hole in an absorbing screen as a function of the distance from the screen in the range of radiation formation length were investigated for the transversal and longitudinal field components. The analysis of the obtained results allows approving the existence of a semi-bare electron with a particularly deprived Coulomb field, which turns into the stable state of the usual electron at the distance of radiation formation length.

PACS 41.60.-m – Radiation by moving charges.
PACS 41.90.+e – Other topics in electromagnetism; electron and ion optics.

1. – Introduction

If a relativistic charged particle with the Lorentz factor γ interacts with a scattering center, the mixed state of the total electromagnetic field (radiation field + particle field) downstream to the interaction point may be observed. At the distance $l_f = \gamma^2\lambda$ (λ is the wavelength of the field Fourier harmonic) this field evolves to a stable state of radiation field and typical charged particle field. In principle the exact solution of the Maxwell equations may be used for description of this process. However, these solutions are often very complicated, or, sometimes, are difficult at the stage of a problem definition. Therefore, phenomenological concepts like *equivalent photons* and *surface current* viewpoint are useful for an intuitive understanding of the main features. The last concept was clearly shown by Bolotovskii in [1], on the example of forward Diffraction Radiation (DR) of a relativistic electron moving near a conductive semi-plane (fig. 1). The travelling Coulomb field (represented by ellipses centered on the successive positions of the particle) induces current in the semi-plane screen, which, in turn, emits DR represented by small pieces of the ellipses. Such radiation field, close to the screen, kills a part of the particle field. The interference gradually disappears (positions 3, 4, 5 of the figure) due to the different velocities, $v \simeq 1 - \gamma^{-2}/2$ and $c = 1$ (in our units), of the Coulomb and radiation fields. These fields get out of phase after a time $t_f \sim \lambda/(c - v) \sim l_f$.

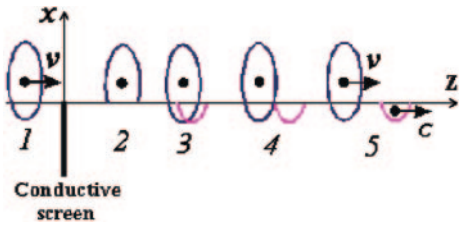

Fig. 1. – Illustration of the radiation formation length effect by Bolotovskii in [1].

"The method of images" is also used to calculate forward and backward TR, and DR [2, 3]. This method comes from electrostatics and is based on both surface charge and surface current concepts.

Another point of view is the equivalent photons method. The Coulomb field is considered as a beam of quasi-real photons. For ultra-relativistic electrons the properties of these photons are very close to the properties of real photons. Namely, the electron field is almost transversal and in the wavelength range from optics to millimeter wavelengths, quasi-real photons are reflected from a mirror, absorbed in the absorber and they do not induce a surface current on a downstream surface of a thick conductive target. There is a region downstream to a conductive or absorbing screen where the Coulomb field is partly missing. In terms of paper [4] this effect is named "shadow effect", and the term "semi-bare electron" has been introduced in [5, 6] to describe a similar effect in the framework of quantum electrodynamics for an electron scattered at a large angle. In both these interpretations the Coulomb field is gradually "repaired" during the formation zone length $l_f \sim \gamma^2 \lambda$.

In [7] the shadowing of an electron Coulomb field by the conductive and absorbing semi-plane in macroscopic mode was investigated. It is remarkable that no principal difference was found in the experiment, whether we use a conductive or absorbing screen for shadowing. Moreover, in [8] it was shown experimentally that the electron field does not induce a surface current on the downstream conductive target surface. Therefore, we may expect that downstream to the absorbing screen A (see fig. 2) the electromagnetic field is defined by the evolution of electron field only.

The experiments presented here are devoted to the investigation of transversal and longitudinal components of electromagnetic field evolution separately inside the formation zone when an electron passes through a hole in an absorbing screen.

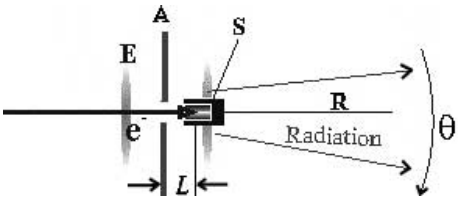

Fig. 2. – A scheme of a possible measurement of the electron electromagnetic field evolution. **E** is the shape of the electron electromagnetic field, **A** is the absorbing screen, **S** is the beam dump.

TABLE I. – *Electron beam parameters.*

Electron energy	6.1 MeV ($\gamma = 12$)	Bunch period	380 ps
Train duration	$\tau \approx 4\,\mu$s	Bunch population	$N_e = 6 \cdot 10^8$
Bunches in a train	$n_b \approx 1.6 \cdot 10^4$	Bunch length	$\sigma \approx 2$ mm

2. – Transversal field evolution investigation

For this purpose we stop the electron beam passing through a hole in an absorbing screen A (fig. 2), inside the beam-dump S, which provides the full absorption of relativistic electrons.

The beam-dump is filled by the millimeter wave radiation absorber, therefore, no radiation in the investigated wavelength region may be emitted by a stopping electron. In frame of the "equivalent photons" viewpoint the shape of electron field flowing around the beam-dump continues evolution, being transformed into real photons. Measuring this radiation in the far-field zone we obtain information about the state of electromagnetic field (electron field + radiation) at the distance L from the screen.

The experiment was performed on the extracted electron beam of the microton of the Tomsk Nuclear Physics Institute (Russia). The beam is extracted from the vacuum chamber through a 20 μm thick beryllium foil. The beam parameters are listed in table I.

The window caused a beam divergence ($\simeq 0.08$ radian). For listed bunch length and population, the electron field and radiation with a wavelength $\lambda > 8$ mm are coherent and radiation intensity is enhanced by 10^8 times. This allows us to measure the radiation using a room-temperature detector. For the radiation measurements we used the detector DP20M, with parameters described in [9]. The detector efficiency in the wavelength region $\lambda = 3 \sim 16$ mm is estimated to be constant up to $\pm 15\%$ accuracy. The detector sensitivity is 0.3 V/mW. A waveguide with a cut-off $\lambda_{\text{cut}} = 17$ mm was used to cut the long-wave background of the accelerator RF system. The high frequency limit of the wavelength interval is defined by the bunch form-factor. This limit ($\lambda_{\min} = 9$ mm) was measured using discrete wave filters [11] and a grating spectrometer.

To exclude the pre-wave zone effect (see [10]) a parabolic telescope was used to investigate the radiation angular distribution (see fig. 3). This method was suggested and tested in [12] and provides the same angular distribution as in the far-field zone ($R \gg \gamma^2\lambda$).

The used absorbing screen provides an absorption in investigated wavelength range by 60 dB, without radiation reflection. The Faraday cup was used for monitoring possible electrons skipping the beam-dump. To exclude a contribution of these electrons in measured characteristics due to a beam divergence, the beam-dump S was placed at a fixed position and changing a screen position provided the variation of distance L. This has limited the maximal value of distance L by 200 mm.

The radiation angular distribution was measured with 1° step for different values of the distance L from 0 to 200 mm with 20 mm step. In fig. 4 the samples of measured angular distribution for different values of distance L are shown.

The full smoothed dependence is presented in fig. 5.

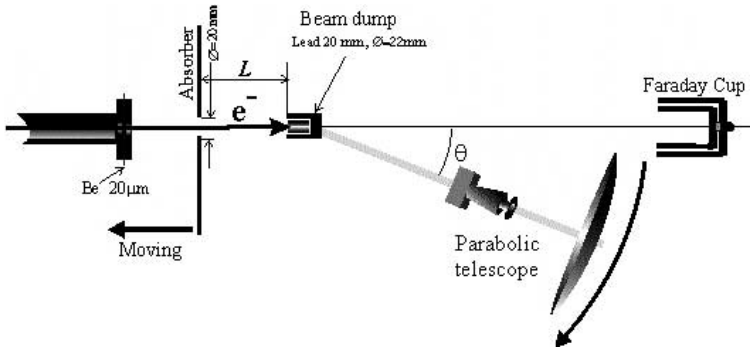

Fig. 3. – Scheme of the experiment.

Unfortunately, the experimental conditions do not allow us the extension of these measurements to $L = \gamma^2\lambda$ (in our case $\gamma^2\lambda \approx 1.5\,\mathrm{m}$) due to the electron beam divergence.

We see in fig. 5 that the electromagnetic field grows when the distance L increases from zero to 200 mm. To explain this effect we cannot use the surface current model like in [1], because according to [7] and [8] no surface current is induced on the downstream surface of thick conductive and absorbing screen. We cannot also use the models, which include the suddenly started and suddenly stopped electron, like in Tamm problem [13] or in case of beta-decay [14], because in our experiment the electron motion is uniform up to absorbing inside the beam-dump.

For theoretical explanation of the observed phenomenon we can use the expression for electromagnetic field of relativistic electron from [14], which is written in terms of the

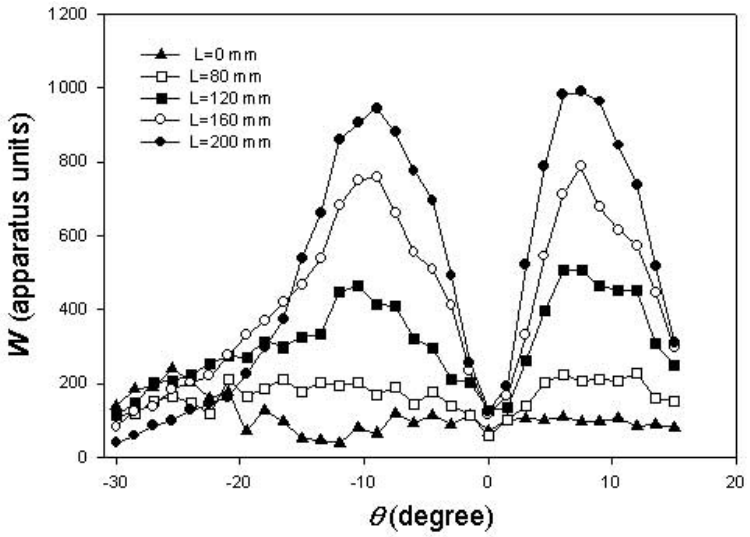

Fig. 4. – Samples of the measured angular distribution of radiation intensity for different distances L between screen and beam dump.

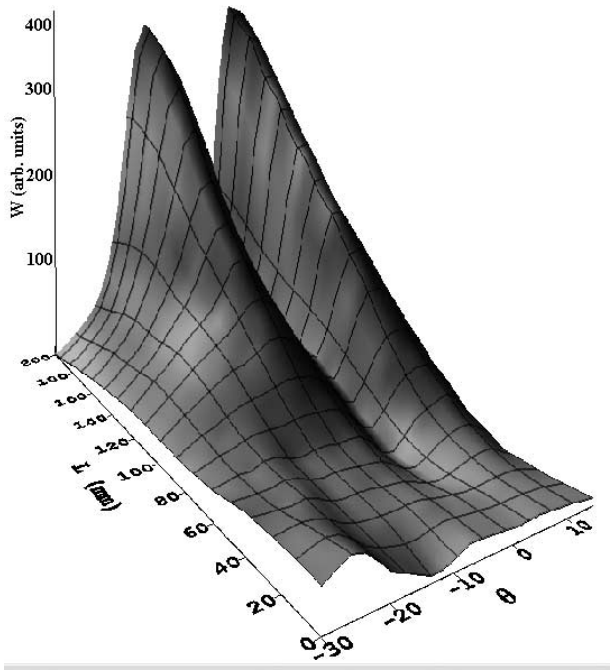

Fig. 5. – The smoothed two-dimensional measured dependence of radiation intensity on the observation angle θ and distance L.

retarded time

$$\vec{E} = \frac{e}{(R - \vec{\beta}\vec{R})^3} \left\{ (1 - \beta^2) \cdot (\vec{R} - \vec{\beta}R) + \vec{R} \times \left((\vec{R} - \vec{\beta}R) \times \vec{\beta}' \right) \right\}, \tag{1}$$

where $\vec{\beta}$ is the electron velocity vector, $\vec{R}$ is the vector from the radiation point to the observation point, e is the electron charge, $\beta = |\vec{\beta}|$, $R = |\vec{R}|$, $\vec{\beta}'$ is the electron acceleration, the light velocity c is assumed to be equal to 1.

According to the experimental conditions the electron motion is uniform with a good accuracy. Therefore $\vec{\beta}' = 0$ and expression (1) can be simplified to the following:

$$\vec{E} = \frac{e \cdot (1 - \beta^2) \cdot (\vec{R} - \vec{\beta}R)}{(R - \vec{\beta}\vec{R})^3}. \tag{2}$$

The value of $\vec{R}$ in (2) should be taken at the time t', which is connected with retarded observation time t by equation $t = t' + R$. In Fourier presentation the field at the distance L from the screen can be presented as

$$\begin{aligned} \vec{E}_\omega &= \int \frac{e \cdot (1 - \beta^2) \cdot (\vec{R} - \vec{\beta}R)}{(R - \vec{\beta}\vec{R})^3} \cdot e^{i\omega t} \mathrm{d}t \\ &= \int \frac{e \cdot (1 - \beta^2) \cdot (\vec{R} - \vec{\beta}R)}{(R - \vec{\beta}\vec{R})^3} \cdot e^{i\omega(t' + R)} \frac{\partial t}{\partial t'} \mathrm{d}t'. \end{aligned} \tag{3}$$

We are interested in the transversal component $\vec{E}_\omega^\perp$ of the electron field. Due to the axial symmetry of the experiment geometry, this component may be presented as

$$\vec{E}_\omega^\perp = \int_0^{L/\beta} \frac{e \cdot (1-\beta^2) \cdot r}{(R - \beta R_\beta)^3} \cdot e^{i\omega(t'+R)} \frac{\partial t}{\partial t'} \mathrm{d}t', \tag{4}$$

where R_β is the component of the vector $\vec{R}$ along the electron velocity $\vec{\beta}$, r is the transversal one and corresponds to the transversal coordinate of the observation point in the cylindrical system; by the definition $R_\beta = L - \beta \cdot t'$, $R = \sqrt{R_\beta^2 + r^2}$. We use here the integration from $t' = 0$ (the output moment from absorber), because according to the pseudo-photon viewpoint the transversal electron field is absorbed in the absorber and for the downstream observer the electron history begins at the moment of output from the absorber with velocity $\vec{\beta}$.

The expression under the integral in (4) is complicated, and integration may be performed only numerically. Using (4) we obtain the electromagnetic field distribution at a distance L from the absorber (see fig. 3), *i.e.* in the plane perpendicular to the electron beam direction at the entrance of the beam dump. The further evolution of the electromagnetic field up to the far-field zone may be calculated using the Kirhoff integral (see [14]) in this plane.

Now we turn to the scheme of experiment in fig. 3. For the angular distribution of radiation downstream to the beam-dump in the far-field zone this integral may be presented as

$$E_\theta = \omega \int_{r_b}^{\infty} E_\omega^\perp \cdot J_1(-\omega \cdot r \cdot \theta) r \, \mathrm{d}r, \tag{5}$$

where J_1 is the Bessel function of the first order.

Taking into account that $\omega = \frac{2\pi}{\lambda}$, we may calculate (see fig. 6) the radiation intensity $W = |E_\theta|^2$ as a function of the observation angle θ and distance L from the screen to the beam-dump for the single electron and for experimental conditions: $\gamma = 12$, $\lambda = 10\,\mathrm{mm}$ (the average wavelength in the experiment).

Comparing figs. 5 and 6 we can see good agreement between experimental and theoretical dependences. Let us remind that in the used theoretical model the concept of suddenly started and suddenly stopped electron was not applied. The observed effect is defined only by evolution of the electron electromagnetic field downstream to the screen. This effect is close to the effect of electron transition from the semi-bare electron to the stable state of the usual electron, considered by Feinberg [5].

3. – Methodical basis for a longitudinal electric field component measurement

Now we should take into account the longitudinal component of the electron field. The electric field of the relativistic electron may be presented in Fourier approximation by the expression

$$\vec{E}_e(\vec{\rho}, z, \lambda) = \begin{Bmatrix} \vec{E}_\perp \\ E_\parallel \end{Bmatrix} = \frac{2e}{\gamma\lambda\beta^2} e^{i\frac{2\pi}{\lambda}z} \begin{Bmatrix} \dfrac{\vec{\rho}}{\rho} K_1\left(\dfrac{2\pi}{\gamma\lambda\beta}\rho\right) \\ -\dfrac{i}{\gamma} K_0\left(\dfrac{2\pi}{\gamma\lambda\beta}\rho\right) \end{Bmatrix}, \tag{6}$$

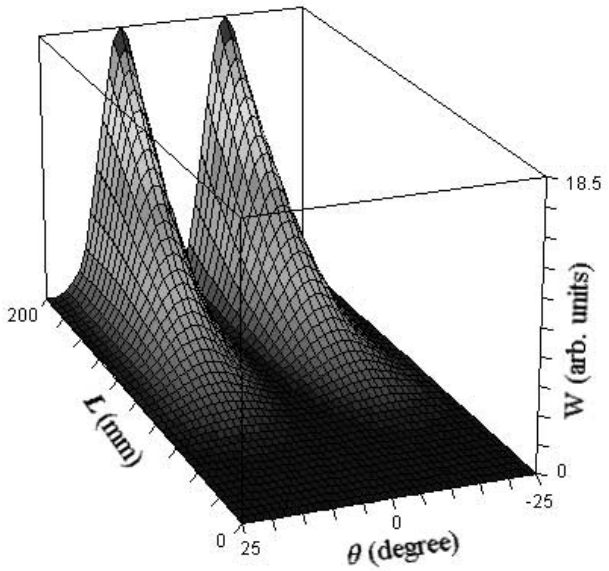

Fig. 6. – Calculated angular distribution of radiation downstream to the beam-dump as a function of the distance between the screen and beam-dump.

where $\vec{E}_e$ is the electron electric strength vector, z is the electron coordinate in the direction of the electron motion with respect to the observation point, $\vec{\rho}$ is the transverse vector of the observation point, $E_\parallel$ is the longitudinal component of the electron electric strength vector and $\vec{E}_\perp$ is the transverse one, λ is the wavelength ($\lambda = \frac{2\pi}{\omega}$, ω is the Fourier approximation variable), e is the electron charge, γ is the Lorenz factor, β is the electron velocity (light velocity is assumed to be equal to 1), K_0 and K_1 are the Bessel functions.

We can see that relation $\frac{E_\parallel^2}{E_\perp^2} \approx \frac{1}{\gamma^2}$ for the relativistic electron is very small (for $\gamma = 12$ $\frac{1}{\gamma^2} = \frac{1}{144}$). It seems that it is impossible to separate longitudinal and transverse components experimentally.

Let us consider the following simple scheme (fig. 7). The electric strength vector of backward transition radiation (BTR) from a conductive target (or backward diffraction

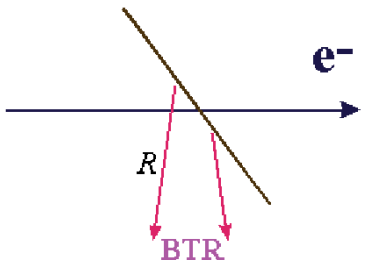

Fig. 7. – Scheme of backward transition radiation.

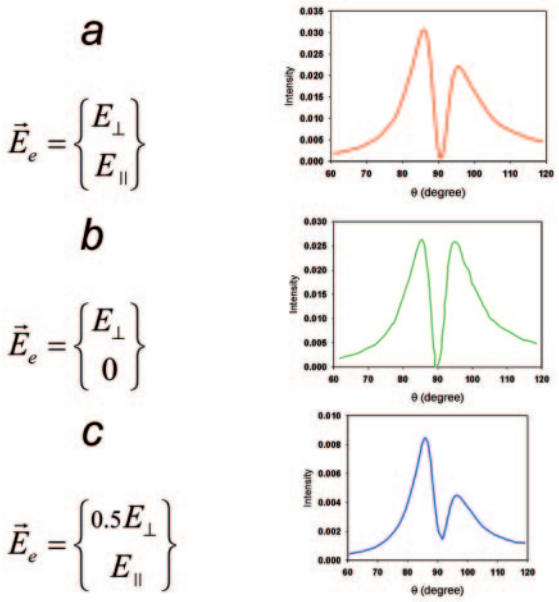

Fig. 8. – BTR asymmetry.

radiation (BDR) of the electron moving through a small hole) may be presented using Kirhgoff integral (7) (see [14]):

$$\vec{E}(\vec{r}) = 2\int_{S_1} (\vec{n} \times \vec{E}_e) \times \mathrm{grad}'\, G \mathrm{d}a', \tag{7}$$

where $G(\vec{r}, \vec{r}') = \frac{1}{4\pi} \cdot \frac{e^{ikR}}{R}$ is the Green's function of a target surface, $\vec{n}$ is the vector perpendicular to the target surface normalized to unit. Using (7) and (6) we may calculate the angular distribution of radiation intensity $|\vec{E}|^2$ in the radiation plane for $\gamma = 12$ in the far-field zone as a function of the observation angle θ (see the case a in fig. 8). We can see in this picture the asymmetry of angular distribution. In order to clarify the cause of this asymmetry, we neglect the longitudinal component $E_\parallel$. In this case (fig. 8, b) the asymmetry disappears. In the opposite case, if we suppress the transversal component $E_\perp$ (see fig. 8, c), the asymmetry is enhanced markedly. Thus, the BTR (or BDR) asymmetry can be used as a sensitive tool for experimental investigation for the longitudinal component of electron electric-field strength.

For measurement of the radiation angular distribution asymmetry we used the scheme shown in fig. 9. The electron beam moves through the hole in the absorbing screen.

The pseudo-photons of the electron field, after shadowing by the screen, are reflected by a thick conductive mirror with a hole for electron beam. This process is a BDR. The mirror is pointed at an angle of 45° to the electron beam direction. The minimum value of distance L is limited by the screen and mirror geometry. To exclude the pre-wave zone effect contribution in this experiment also the parabolic telescope was used for a BDR angular distribution measurement. To exclude the transverse beam size contribution in BDR, the position of the conductive target was fixed and the distance L was varied by the variation of the absorber position.

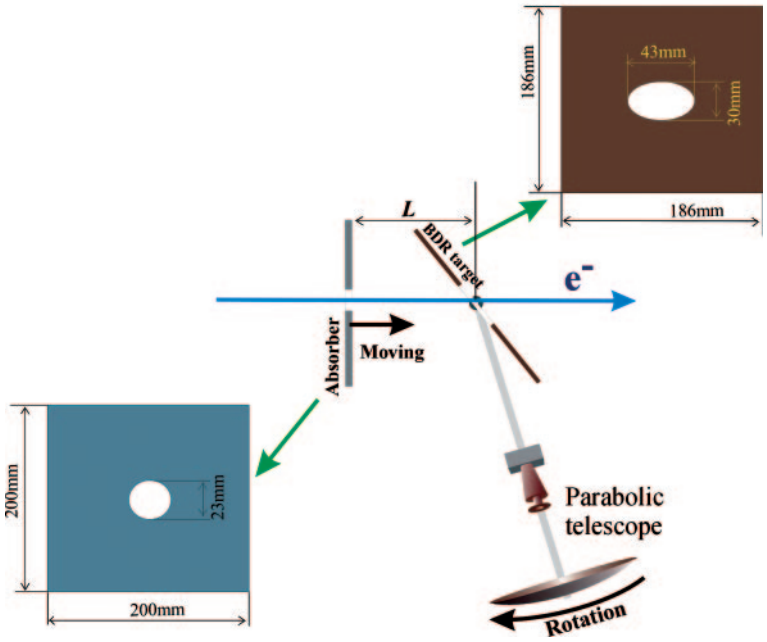

Fig. 9. – Scheme of experiment.

The measurements were performed with 1 degree step in angular distribution and with 20 mm step in distance L. The statistical error of measured radiation intensity is $\sigma \approx 5\%$. In fig. 10 is shown the smoothed measured dependence of the radiation intensity on the observation angle θ and distance L.

Using this dependence we may obtain the asymmetry $\eta = \frac{M_1 - M_2}{M_1 + M_2}$ as a function of distance L (see fig. 11), where M_1 and M_2 are the values of the radiation intensity in the left and right maximum of the angular distribution for a fixed value of L.

As was shown above, due to $E_{\parallel}^2 \ll E_{\perp}^2$ the main contribution in the average radiation intensity ($(M_1 + M_2)/2$) is provided by the transversal component of the electron field. Therefore we may expect that the shadowing effect depend mainly on this component. To check this supposition we chose the following model. Let us introduce in (6) the suppression factor α, which depends on L (see (8)).

$$\vec{E}_e(\vec{\rho}, z, \lambda) = \begin{Bmatrix} E_{\perp} \\ E_{\parallel} \end{Bmatrix} = \frac{2e}{\gamma\lambda\beta^2} e^{i\frac{2\pi}{\lambda}z} \begin{Bmatrix} \alpha\dfrac{\vec{\rho}}{\rho} K_1\left(\dfrac{2\pi}{\gamma\lambda\beta}\rho\right) \\ -\dfrac{i}{\gamma} K_0\left(\dfrac{2\pi}{\gamma\lambda\beta}\rho\right) \end{Bmatrix}. \tag{8}$$

From (8) for $E_{\parallel}^2 \ll E_{\perp}^2$ (as shown above),

$$(M_1 + M_2)/2 \sim q\alpha^2, \tag{9}$$

where q is the proportional factor. Using (8) we may calculate the asymmetry as a

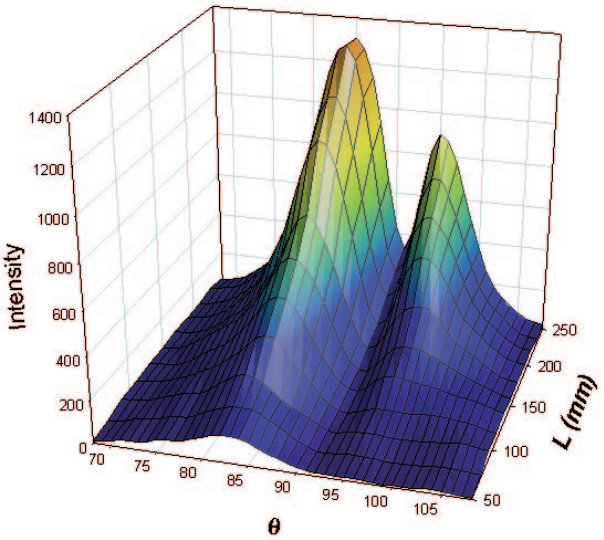

Fig. 10. – Smoothed experimental dependence of BDR.

function of α^2 (solid line in fig. 12). On the other hand, using data from dependence shown in fig. 10 and taking into account (9) we can obtain the experimental dependence of the measured asymmetry on α^2 with accuracy of the proportional factor q, which is undefined. We may found this factor performing the fit of the experimental data to theoretical dependence by factor q. The dotted line in fig. 12 is the fit of experimental data to theoretical dependence.

We can see good agreement between theoretical calculation and experimental results. It is therefore concluded that the model where the longitudinal component of relativistic electron field does not depend on the distance between screen and BDR target is in good agreement with experiment. In contrast the dashed line in fig. 12 corresponds to the

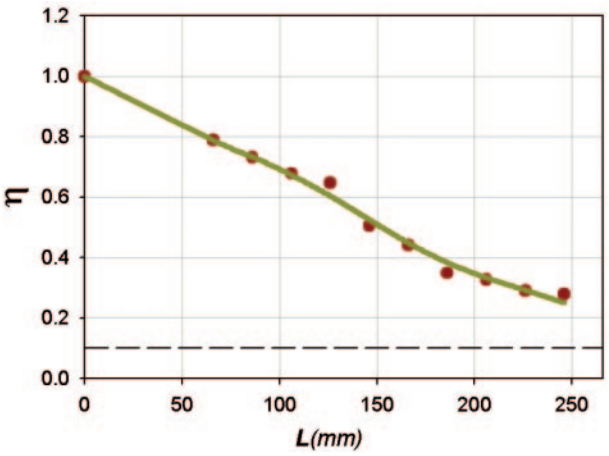

Fig. 11. – Asymmetry as a function of distance L.

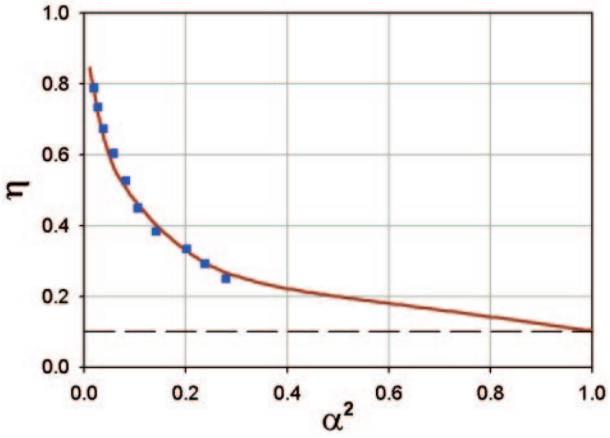

Fig. 12. – Dependence of the asymmetry on the suppression factor α. Dots are the experimental points. Solid line is the fit of the theoretical dependence to the experimental data.

case when transversal and longitudinal components of the electron field are shadowed proportionally.

From the above reasoning it is clear that in contrast with the transversal component of the electron field, the shadowing effect is not shown for the longitudinal component in interactions with the absorbing screen.

* * *

This work was partly supported by the warrant-order 1.226.08 of the Ministry of Education and Science and by contract 02.740.11.0245 of Ministry of Education and Science of the Russian Federation.

REFERENCES

[1] Bolotovskii B. N., Preprints of Lebedev Institute of Physics, Soviet Academy of Sciences, Vol. **140** p. 95.
[2] Ginzburg V. L. and Tsitovich V. N., *Transition Radiation and Transition Scattering* (Science, Moskow) 1983.
[3] Bolotovskii B. M. and Serov A. V., *Phys. Usp.*, **52** (2009) 487.
[4] Artru X. and Ray C., *Interferences between light emitted by charged particles crossing or skimming past optic fibers*, in *International Symposium RREPS'07, Prague, 2007.*
[5] Feinberg E. L., *Sov. Phys. Ups.*, **22** (1979) 479.
[6] Shul'ga N. F. and Syshchenko V. V., *J. Phys. At. Nucl.*, **63** (2000) 2018.
[7] Naumenko G. A., Potylitsin A. P., Sukhikh L. G., Popov Yu. A. and Shevelev M. V., *JETP Lett.*, **90** (2009) 96.
[8] Naumenko G., Potylitsyn A., Popov Yu., Sukhikh L. and Shevelev M., *J. Phys.: Conf. Ser.*, **236** (2010) 012024.
[9] Kalinin B. N., Naumenko G. A., Potylitsyn A. P. *et al.*, *JETP Lett.*, **84** (2006) 110.
[10] Hanke K., CLIC note 298, 19.04.1996.
[11] Verzilov V. A., *Phys. Lett. A*, **273** (2000) 135.
[12] Kalinin B. N., Naumenko G. A., Potylitsyn A. P. *et al.*, *JETP Lett.*, **84** (2006) 110.
[13] Tamm I. E., *J. Phys. USSR*, **1** (1939) 439.
[14] Jackson J. D., *Classical Electrodynamics*, 3rd edition (J. Wiley & Sons, New-York) 1998.